

Mesh-MLP: An all-MLP Architecture for Mesh Classification and Semantic Segmentation

Qiujie Dong, Xiaoran Gong, Rui Xu, Zixiong Wang, Shuangmin Chen, Shiqing Xin, Changhe Tu, Wenping Wang

Shandong University, Nankai University, Qingdao University of Science and Technology, Texas A&M University



Figure 1: A gallery of segmentation results of the COSEG dataset. From left to right: Tele-aliens, Chairs, and Vases.

Abstract

With the rapid development of geometric deep learning techniques, many mesh-based convolutional operators have been proposed to bridge irregular mesh structures and popular backbone networks. In this paper, we show that while convolutions are helpful, a simple architecture based exclusively on multi-layer perceptrons (MLPs) is competent enough to deal with mesh classification and semantic segmentation. Our new network architecture, named Mesh-MLP, takes mesh vertices equipped with the heat kernel signature (HKS) and dihedral angles as the input, replaces the convolution module of a ResNet with Multi-layer Perceptron (MLP), and utilizes layer normalization (LN) to perform the normalization of the layers. The all-MLP architecture operates in an end-to-end fashion and does not include a pooling module. Extensive experimental results on the mesh classification/segmentation tasks validate the effectiveness of the all-MLP architecture.

CCS Concepts

• Computing methodologies → Shape analysis;

1. Introduction

Convolutional neural networks (CNNs) [RDGF16, DBK*21] have achieved great success in computer vision, which benefits from the regular grid structure of images and allows flexible network design. The success of CNNs also sparks a rising interest in geometric deep learning that takes 3D data as the input. However, 3D data has various representation forms and thus one has to design networks for a specific kind of representation form. For example, the deep neural networks designed for triangle meshes [HHF*19] and those for point clouds [QSMG17, QYSG17, LBS*18] are quite different. Generally

speaking, polygonal surfaces are more informative and less ambiguous than point clouds, but the irregular connections between mesh vertices cause difficulty in network design. Because of this, there are many research works [SMKLM15, HHF*19, HJZS20, HLG*22, SACO22, DWL*23] that regularize mesh-based inputs to adapt to the requirements of the popular deep convolutional networks or specifically designed for triangular meshes, which are challenging tasks.

MVCNN [SMKLM15] and MVRNN [LBD17] need to convert the meshes into multi-view images before being fed into the neural

network so that 2D CNNs can be used directly. MeshCNN [HHF*19] defines the convolutional operator based on the observation that each mesh edge has four neighboring edges. In this way, it encodes the edge-centered features. CurvaNet [HJZS20] encodes the vertex-wise feature by normalizing the directional curvatures into a set of M -dimensional vectors. SubdivNet [HLG*22] first preprocesses a coarse mesh into a fine version using the Loop subdivision algorithm so that the mesh-based convolution kernel pattern can work based on regular adjacency. Laplacian2Mesh [DWL*23] advocates performing mesh classification/segmentation tasks in the spectral domain. It does not care about the mesh irregularity, but it requires a tedious preprocessing step.

In this paper, we propose *Mesh-MLP* for mesh classification and segmentation, a new neural network consisting exclusively of MLPs. The network takes the mesh vertices equipped with the features at your fingertips as the input. To be more specific, the heat kernel signature (HKS) and dihedral angles are kept at each vertex. There are two key points in architectural design. On the one hand, we replace the convolution module of a ResNet with Multi-layer Perceptron (MLP). In order to perform different tasks, e.g., mesh classification and semantic segmentation, it suffices to link different head blocks to the output of the basic backbone. Additionally, considering that the meshes in a dataset may have varying numbers of vertices, we set the batch size to 1 and use gradient accumulation [HSM17] to virtually increase the batch size. However, it's also worth noting that padding or truncation of mesh data can alleviate this issue, but at the cost of information redundancy or loss. As reported in [VSP*17], the Batch Normalization (BN) [Iof17] cannot get stable statistics when the batch size is 1. In order to tackle the issue, we use Layer Normalization (LN) [BKH16] instead to accomplish data normalization.

Compared with those carefully designed networks, our all-MLP network consists of easily available modules and does not need a convolution operator at all. It is able to deal with a mesh with any resolution and any triangulation. We perform comprehensive experiments to validate the effectiveness of the proposed Mesh-MLP on shape classification and semantic segmentation tasks. First, the comparison statistics show that our Mesh-MLP outperforms the state-of-the-art on average. Second, our network requires only a small preprocessing cost and converges fast. Finally, our approach is insensitive to mesh resolution and meshing quality.

2. Related Work

In this section, we first briefly review the geometric learning works that represent a 3D shape by multi-view images, voxels, and so on. We then review surface-based neural networks where one has to define a convolutional operator to adapt to the irregular mesh structure.

2.1. 3D Shape Deep Learning

Various representation forms have been proposed to describe the 3D shape, such as multi-view images, point clouds, triangle meshes, voxels, and so on. Inspired by pixelated images, Wu et al. [WSK*15] proposed to transform an input object into voxels so that a 3D convolutional operator can be easily defined. In this way, their approach

can be used in many applications, such as alignment [HFW*19] and semantic segmentation [TCA*17]. One of the bottlenecks of the voxelization representation lies in the cubically increasing complexity of memory usage, as well as the corresponding computation cost. In order to tackle this issue, the octree-based volumetric representation [RUG17, WSLT18] has been proposed. However, it requires the designer to carefully design an octree adaptive convolutional operator. There are many research works [SMKLM15, LBD17] that render a 3D shape as multi-view images so as to facilitate deep learning via 2D CNNs. However, this kind of technique cannot deal with highly curved objects since there are some parts invisible to users. With the development of autonomous driving, point clouds have also become a popular representation in 3D shape deep learning. To extract the features of point clouds, PointNet [QSMG17] and PointNet++ [QYSG17] build the spatial correlations between points with KNN search. PointCNN [LBS*18] proposes to learn an χ -transformation from the input points to permute the points into a latent and potentially canonical order. PCT [GCL*21] takes point clouds as the input and introduces the transformer mechanism to improve the performance. However, point clouds are less informative than mesh surfaces and are sometimes ambiguous in inferring the geometry features.

2.2. Mesh Based Deep Learning

Generally speaking, the design of a mesh-based deep learning network is two-fold. First, one has to define how the geometric feature at a primitive (a vertex, an edge, or a face) is produced. CurvaNet [HJZS20] defines a per-vertex feature by discretizing the directional curvatures into M -dimensional vector. MeshWalker [LT20] uses random walks to explore the mesh topology. It is able to encode the localized features but requires a large computational cost as the mesh resolution increases. Second, the mesh-based deep learning network has to define some key modules including the convolution operation and the pooling operation. MeshCNN [HHF*19] is inspired by the wedge structure of a manifold mesh surface, i.e., each edge is correlated with four edges belonging to the two neighboring triangular faces. The pooling operation of MeshCNN is thus defined by the edge-collapse operation. PD-MeshNet [MLR*20] encodes the adjacency between faces by the primal and dual graph. The pooling operation of PD-MeshNet is based on the mesh simplification algorithm. SubdivNet [HLG*22] gives a special CNN for 2-manifold meshes to aggregate local features from nearby faces. However, the triangle meshes need to be pre-processed by the Loop subdivision algorithm before being fed into the SubdivNet. Recently, it becomes popular to use Laplacian to implicitly express the geometry and topology of the meshes. Benefiting from the eigendecomposition in the differentiable pipeline, HodgeNet [SS21] proposes a spectral-based learning technique. Very recently, Laplacian2Mesh [DWL*23] transforms the features of vertices from Euclidean space to Laplacian space. All the aforementioned methods have to design special convolutional operations to bridge irregular mesh structures and popular backbone networks.

DiffusionNet [SACO22], also belonging to the spectral-based learning approaches, uses the spectral acceleration technique to get the local-to-global features of the vertices. DiffusionNet consists of a sequential list of MLP blocks, and works without any CNN

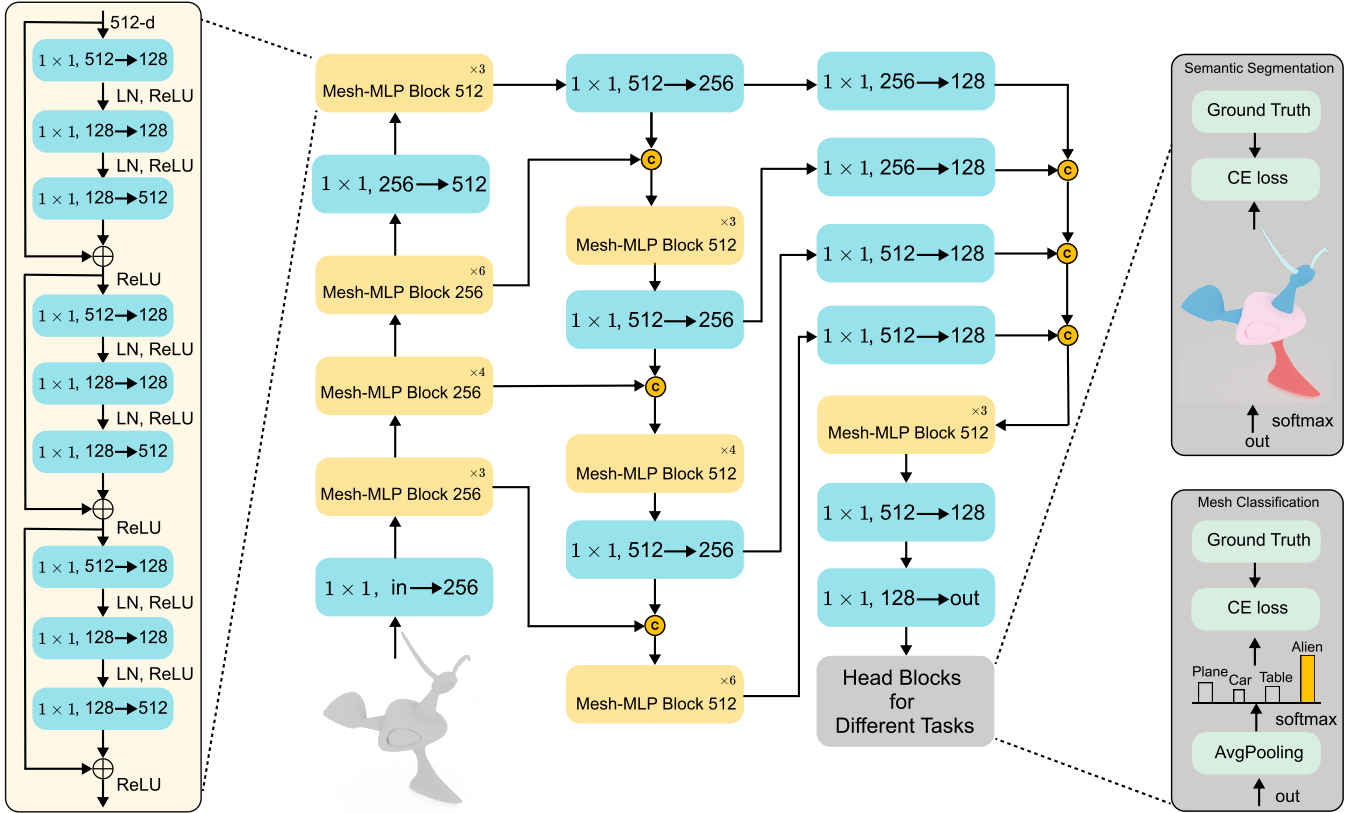


Figure 2: Our network pipeline for coping with the mesh classification and segmentation tasks. All MLP layers constitute our network structure. As can be seen from the expanded view (on the left) of the Mesh-MLP Block, we continue to use the bottleneck structure, which can effectively reduce the amount of computation. The circled “C” denotes the concatenation operation, and the circled “+” denotes the sum operation. The number in the upper right corner of the Mesh-MLP Block indicates that there are serial blocks corresponding to the number. For example, the picture on the left is composed of three 512-dimensional Mesh-MLP blocks. The blocks with a blue background represent the fully connected layer of 1×1 , the left side of the arrow represents the input dimension, and the right side represents the output dimension.

modules, which shows that the all-MLP architecture is a choice in 3D shape understanding. In this paper, we further explore the potential of the all-MLP architecture. The difference lies in that we borrow the key spirits of ResNet and U-Net, allowing the network to learn more high-level semantic features.

3. Methodology

3.1. Key Modules in the all-MLP Architecture

Input Features. Existing research works [HHF*19, HLG*22, SACO22, DWL*23] show that using hand-crafted shape descriptors to define the geometric feature helps improve the overall performance of the network. Generally, both intrinsic shape descriptors (for characterizing shape variations) and extrinsic shape descriptors (for encoding coordinate-dependent properties) are necessary to form the geometric feature. In this paper, we define the per-vertex feature by considering three kinds of shape descriptors including (1) the heat kernel signature (HKS) [SOG09], (2) vertex coordinates and normals, and (3) dihedral angles.

The HKS can not only encode the local-to-global shape vari-

ations but also implicitly represent the topology information of the input triangle mesh. It is widely used in geometric deep learning [DWL*23, SACO22]. The 3-dimensional vertex coordinates and the 3-dimensional vertex normal encode the coordinate-dependent information and have been widely used in [DWL*23, QGY*22]. Besides, the per-vertex dihedral angle is computed by distributing the dihedral angle of a mesh edge to its endpoints, which is shown to be very useful in Laplacian2Mesh [DWL*23]. It’s worth noting that users can add some task-specific features to augment the input by a simple concatenation.

Network Architecture. As shown in Figure 2, our Mesh-MLP resembles the U-Net [RFB15], which uses the mirror structure that connects the encoding features and decoding features in the same resolution via the skip connection at each level. The main difference between ours and the original U-Net [RFB15] network is that we use the ResNet [HZRS16] block as the unit of our Mesh-MLP. Additionally, we concatenate the outputs at different up-sampling stages for aggregating multi-resolution information, which enables our network to learn more discriminative features.

In computer vision, ResNet [HZRS16] is a powerful framework

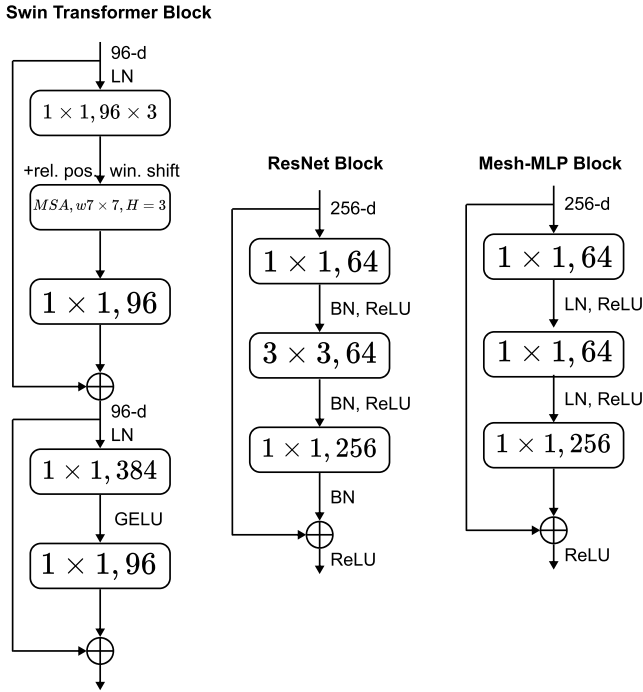


Figure 3: The designs for a Swin Transformer Block, a ResNet Block, and a Mesh-MLP Block. Complex Swin Transformer Block needs to add specialized modules in the network structure and connect two residual blocks in series. Although Resnet Block and Swin Transformer Block perform well on tasks for 2D images, their performance on 3D data is poor.

with residual learning. Here, we use a network structure similar to ResNet Block as the building blocks of our Mesh-MLP (see Figure 3), where each convolution layer is replaced by MLP. The main purpose of placing ReLU [GBB11] after the MLP layers are to introduce the property of nonlinearity to make the model more expressive.

Gradient Accumulation. The 3D shapes in the same dataset may have different numbers of vertices, which prevents one from using large batch sizes in the network. Therefore, some typical techniques, such as padding, truncation, or function map [DWL*23], are used to pre-process the feature matrices before inputting them into the network. But such techniques may cause information redundancy or loss. In this paper, we set the batch size to 1 and use gradient accumulation [HSM17] for purpose of achieving the same performance as a large batch size. Note that gradient accumulation is a commonly used technique to split the batch of samples into several min-batches of samples. The min-batches of samples are processed sequentially and the gradients are accumulated after a certain number of min-batches have been performed.

Layer Normalization. BN [Iof17], commonly used in the original ResNet [HZRS16] blocks, is crucial to reduce over-fitting and improve convergence. But BN does not help under the situation that the batch size is 1. Inspired by Transformers [VSP*17], we substi-

tute the simpler LN [BKH16] for the BN in the original ResNet since LN is independent of the batch size (see Figure 3).

3.2. Shape Classification

The pooling layer is to reduce the dimension of the feature map, enabling the network to learn the features of the meshes from local to global. Pooling is an indispensable component in most of the previous learning methods [HHF*19, HLG*22]. The pooling operation is mostly designed based on the mesh simplification methods [HHF*19, HLG*22, MLR*20]. However, the HKS, as a part of input features to our Mesh-MLP, has encoded the local-to-global shape variations. Therefore, our network does not include the pooling component, which can prevent Mesh-MLP from causing additional information loss. Only when we conduct the mesh classification task, a simple averaging pooling is enforced so as to get a $1 \times c$ vector, where c is the number of classes.

3.3. Shape Segmentation

Different from the shape classification task, the task of shape segmentation does not need a pooling operation. Note that the output of the Mesh-MLP, when conducting shape segmentation, is a vector consisting of the per-vertex labels. The per-vertex labels can be then translated into per-face labels by simply averaging the probability in which the vertex belongs to a surface patch.

After that, for each face f , we extract the labels of the 1-ring neighboring faces (has at least one common vertex with f). By counting the labels in the 1-ring neighborhood, we assign the label with the highest frequency to f . In fact, the graph-cuts operation serves as a post-processing step in many existing shape segmentation approaches. To our knowledge, the regularization ability of the graph-cuts operation is too strong, and thus it is unfair to take the graph-cuts results for comparison.

4. Experiments

We present extensive experiments to validate the effectiveness of simple Mesh-MLP on mesh classification and semantic segmentation tasks. All the meshes we used are scaled into a unit scale. During the training phase, we select one Euler angle among $0, \pi/2, \pi$ to perform data augmentation, where the rotation axis is the x -axis, the y -axis or the z -axis.

4.1. Mesh Classification

We conduct the mesh classification experiment on the SHREC-11 dataset [LGB*11], which consists of 30 classes, with 20 examples per class. Following the setting proposed by [ESKBC17], all methods are evaluated based on the 10-10 and 16-4 train-test split, respectively. Each 3D shape in the original dataset [LGB*11] has over 18k faces of the mesh and only 500 faces in the simplified dataset [HHF*19].

Following the most related works, we test our method on the simplified SHREC-11 dataset. As shown in Table 1, our Mesh-MLP outperforms the others on both train-test splits. Note that Mesh-MLP also gets the best performance on the original dataset, in

which classification accuracy statistics are 100% on the split-16 and 99.7% on the split-10.

Table 1: The classification accuracy statistics on the SHREC11 dataset [HHF*19]. Each dataset contains two experiments, split-16 with 16 models for training and split-10 with 10 models for training. The bold fonts indicate the best performance.

Method	Split-16	Split-10
GWCNN [ESKBC17]	96.6%	90.3%
MeshCNN [HHF*19]	98.6%	91.0%
PD-MeshNet [MLR*20]	99.7%	99.1%
MeshWalker [LT20]	98.6%	97.1%
SubdivNet [HLG*22]	99.9%	99.5%
HodgeNet [SS21]	99.2%	94.7%
DiffusionNet [SACO22]	–	99.5%
Mesh-MLP (ours)	100%	99.7%

4.2. Mesh Semantic Segmentation

We demonstrate the ability of Mesh-MLP for semantic segmentation using COSEG dataset [WAvK*12], human body dataset [MGA*17] and Intra dataset [YXKI20]. The goal of semantic segmentation is to predict the per-face segmentation labels. We use the “hard” labels [MLR*20] that measure face-wise accuracy to define the evaluation indicator, instead of the “soft” labels [HHF*19] with edge-wise accuracy.

COSEG. The COSEG dataset includes three shape datasets: Chairs, Vases, and Tele-aliens containing 400, 300, and 200 triangle meshes, respectively. The meshes in the Vases dataset and the Tele-aliens dataset are labeled into 4 parts, and 3 parts in the Chairs dataset. As in MeshCNN [HHF*19], we randomly split the dataset into an 85%-15% train-test.

The quantitative results are shown in Table 2. In Chairs and Vases datasets, our Mesh-MLP achieves state-of-the-art performance and obtains comparable results in Tele-aliens class. Because there are a large number of long and narrow triangles in this dataset, it is beneficial to MeshCNN [HHF*19] and HodgeNet [SS21], both of which use the per-edge features as the part of input features. The semantic segmentation results are visualized in Figure 1.

Human Body Segmentation. We also evaluate the performance of our Mesh-MLP on the human body dataset, which consists of 370

Table 2: The mesh segmentation accuracy statistics on the COSEG dataset [WAvK*12].

Method	Chairs	Vases	Tele-aliens
PointNet [QSMG17]	70.2%	91.5%	54.4%
DCN [XDZ17]	95.7%	90.9%	-
MeshCNN [HHF*19]	93.0%	92.4%	96.3%
HodgeNet [SS21]	95.7%	90.3%	96.0%
Laplacian2Mesh [DWL*23]	96.6%	94.6%	95.0%
Mesh-MLP (ours)	97.5%	95.1%	95.9%

Table 3: The mesh segmentation accuracy statistics on the Human-Body dataset [MGA*17].

Method	Input	Accuracy
PointNet [QSMG17]	point cloud	74.7%
PointNet++ [QYSG17]	point cloud	82.3%
MeshCNN [HHF*19]	mesh	85.4%
PD-MeshNet [MLR*20]	mesh	85.6%
HodgeNet [SS21]	mesh	85.0%
Laplacian2Mesh [DWL*23]	mesh	88.6%
Mesh-MLP (ours)	mesh	90.6%

training 3D shapes from Adobe Fuse [Ado16], FAUST [BRLB14], MIT [VBMP08], and SCAPE [KL17]. The test set has 18 3D shapes from SHREC07 [GBP07] humans dataset. All the meshes are labeled by Maron et al. [MGA*17] and manually segmented into 8 parts. Most approaches use the same version of this dataset processed by MeshCNN [HHF*19] which downsamples the per mesh to 1500 faces.

As shown in Table 3, we report the accuracy statistics of various methods, and our Mesh-MLP outperforms the other approaches. The approaches we compare require complex pre-processing such as re-meshing triangle-meshes [HHF*19], building the primal-dual graphs [MLR*20], and computing eigen-decomposition [SS21, DWL*23]. From the qualitative results (see Figure 4), we can see that our method has the ability to perform accurate and consistent part segmentation on the human body.

Intra. We evaluate our Mesh-MLP in the medical dataset. Intra has 116 annotated samples [YXKI20] for the binary part segmentation task [YZW*21] since the boundary lines are grouped into the aneurysm class. These aneurysm segments are divided and annotated manually by medical experts and the scale of each aneurysm segment is based on the need for a preoperative examination [YXKI20].

In Table 4, We report the performance using the Point Intersection over Union (IoU) and Sørensen–Dice coefficient (DSC) as the evaluation metrics. All methods apply 512 input points, and our Mesh-MLP achieves the best results for parent vessel segmentation on IoU and DSC. To further evaluate our method, we qualitatively

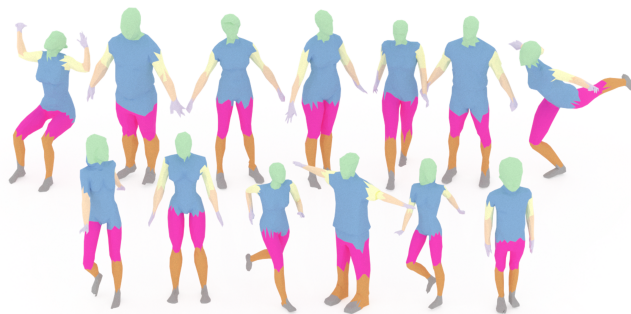
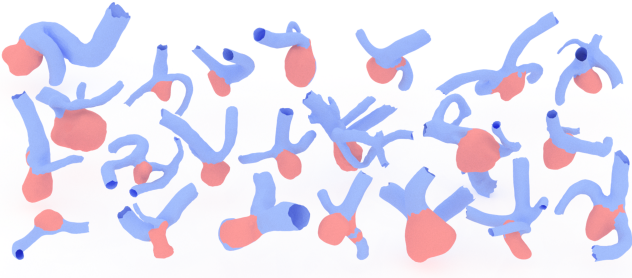


Figure 4: We test the dataset of the Human Body and visualize the segmentation result for the models.

Table 4: The mesh segmentation accuracy statistics on the Intra dataset [YXKI20]. “vessel” and “aneurysm” represent parent vessel segments and aneurysm segments.

Method	IoU		DSC	
	vessel	aneurysm	vessel	aneurysm
PointNet [QSMG17]	74.0%	37.3%	84.1%	49.0%
PointNet++ [QYSG17]	93.4%	76.2%	96.5%	83.9%
PointCNN [LBS*18]	92.5%	70.7%	96.0%	78.6%
SO-Net [LCL18]	94.2%	80.1%	97.0%	87.9%
SpiderCNN [XFX*18]	90.2%	67.3%	94.5%	75.8%
PointConv [WQF19]	94.2%	79.1%	96.9%	86.0%
GS-Net [XZQ20]	90.1%	64.5%	94.6%	74.5%
PCT [GCL*21]	92.5%	78.1%	96.1%	85.8%
AdaptConv [ZFF*21]	90.5%	70.3%	96.0%	80.6%
PACConv [XDZQ21]	92.0%	78.7%	95.7%	87.6%
3DMedPT [YZW*21]	94.8%	81.8%	97.3%	89.3%
Mesh-MLP (ours)	95.2%	87.7%	97.5%	93.0%

**Figure 5:** The segmentation results of intracranial aneurysm show that our method achieves accurate results.

evaluate Mesh-MLP in Figure 5, which exhibits superiority in segmenting medical data.

4.3. Ablation Studies

We conduct ablation experiments on network structure, input features, and normalization. Ablation experiments can identify which are critical for the network to make accurate predictions.

Convolution Patterns Network design is a critical part of deep learning. As shown in Table 5, we start with the original U-Net architecture that with fully convolutiona (Conv) and gradually leverage the modern design modules such as ResNet (Conv + Res). The combination of MLP with residual learning (MLP + Res) gets the best results. It should mention that U-Net with pure MLP does not work well in our tasks.

Input Features We also conduct experiments to show the effectiveness of the input features for each vertex in Table 6. Among them, HKS plays an important role in our task since it encodes the local-to-global shape variations and the topology information of the input.

Normalization Normalization techniques are an essential component of many neural network architectures. We revisit the different

Table 5: The mesh segmentation accuracy statistics for different network structures.

Backbone	Human-Body	Tele-aliens	Chairs
UNet (Conv)	84.0%	94.0%	96.6%
UNet (Conv + Res)	88.2%	94.1%	96.7%
UNet (MLP + Res)	90.6%	95.9%	97.5%
UNet (MLP)	25.2%	31.3%	35.8%

Table 6: The mesh segmentation accuracy statistics for different input features.

Input Features	Human-Body	Tele-aliens	Vases
Vertex coordinates	70.3%	65.0%	85.7%
+ Vertex normal	76.5%	77.4%	93.3%
+ dihedral angle	83.1%	87.1%	93.7%
+ HKS (full)	90.6%	95.9%	95.1%

impacts of normalization techniques in our task, as shown in Table 7. Note that directly leveraging LN in the original ResNet will result in suboptimal performance [WH18], but we observe that LN is most suitable for our Mesh-MLP that gets the best performance.

Table 7: The mesh segmentation accuracy statistics for different Normalizations.

Normalization	Human-Body	Chairs
Batch Norm [Iof17]	85.4%	85.8%
Group Norm [WH18]	87.0%	96.9%
Global Response Norm [WDH*23]	87.0%	95.5%
Instance Norm [UVL16]	88.5%	96.9%
Layer Norm [BKH16]	90.6%	97.5%

5. Conclusion

We revisit the related works for mesh-understanding tasks and present an all-MLP neural network for mesh classification and semantic segmentation. In our Mesh-MLP, we do not require tedious and time-consuming pre-processing to process input data. At the same time, we do not need to design a dedicated network structure to deal with the irregularities of the mesh structure. The ResNet block is used as the constituent unit of the U-net architecture, and all convolution operations in the original block are replaced by simpler MLPs. LN is chosen to implement the normalization of the layers. Extensive experimental results show that the Mesh-MLP, being amazingly simple, can produce competitive results.

Limitations. The Mesh-MLP uses HKS to keep the topology clues. For a disconnected object, however, the HKS cannot encode the positional relationship between disconnected components, which may lead to unreliable results.

Future Work. The Mesh-MLP is a simple yet effective neural network that can be applied to perform mesh understanding tasks. We believe that it can stimulate more follow-up research works. In the future, we shall explore the possibility of building a large all-MLP network to make the model more expressive.

References

- [Ado16] ADOBE: Adobe fuse 3d characters. <https://www.mixamo.com>, 2016. 5
- [BKH16] BA J., KIROS J. R., HINTON G. E.: Layer normalization. *ArXiv abs/1607.06450* (2016). 2, 4, 6
- [BRLB14] BOGO F., ROMERO J., LOPER M., BLACK M. J.: Faust: Dataset and evaluation for 3d mesh registration. *2014 IEEE Conference on Computer Vision and Pattern Recognition* (2014), 3794–3801. 5
- [DBK*21] DOSOVITSKIY A., BEYER L., KOLESNIKOV A., WEISENBERG D., ZHAI X., UNTERTHINER T., DEGHANI M., MINDERER M., HEIGOLD G., GELLY S., USZKOREIT J., HOULSBY N.: An image is worth 16x16 words: Transformers for image recognition at scale. *ArXiv abs/2010.11929* (2021). 1
- [DWL*23] DONG Q., WANG Z., LI M., GAO J., CHEN S., SHU Z., XIN S., TU C., WANG W.: Laplacian2mesh: Laplacian-based mesh understanding. *IEEE Transactions on Visualization and Computer Graphics* (2023), 1–13. 1, 2, 3, 4, 5
- [ESKBC17] EZUZ D., SOLOMON J. M., KIM V. G., BEN-CHEN M.: Gwenn: A metric alignment layer for deep shape analysis. *Computer Graphics Forum* 36 (2017). 4, 5
- [GBB11] GLOROT X., BORDES A., BENGIO Y.: Deep sparse rectifier neural networks. In *International Conference on Artificial Intelligence and Statistics* (2011). 4
- [GBP07] GIORGI D., BIASOTTI S., PARABOSCHI L.: Shape retrieval contest 2007: Watertight models track. *SHREC competition 8*, 7 (2007), 7. 5
- [GCL*21] GUO M.-H., CAI J., LIU Z.-N., MU T.-J., MARTIN R. R., HU S.: Pct: Point cloud transformer. *Comput. Vis. Media* 7 (2021), 187–199. 2, 6
- [HFW*19] HANOCKA R., FISH N., WANG Z., GIRYES R., FLEISHMAN S., COHEN-OR D.: Alignet: Partial-shape agnostic alignment via unsupervised learning. *ACM Trans. Graph.* 38 (2019), 1:1–1:14. 2
- [HHF*19] HANOCKA R., HERTZ A., FISH N., GIRYES R., FLEISHMAN S., COHEN-OR D.: Meshcnn: a network with an edge. *ACM Transactions on Graphics (TOG)* 38 (2019), 1–12. 1, 2, 3, 4, 5
- [HJZS20] HE W., JIANG Z., ZHANG C., SAINJU A. M.: Curvnet: Geometric deep learning based on directional curvature for 3d shape analysis. *Proceedings of the 26th ACM SIGKDD International Conference on Knowledge Discovery & Data Mining* (2020). 1, 2
- [HLG*22] HU S.-M., LIU Z.-N., GUO M.-H., CAI J.-X., HUANG J., MU T.-J., MARTIN R. R.: Subdivision-based mesh convolution networks. *ACM Trans. Graph.* 41, 3 (mar 2022). 1, 2, 3, 4, 5
- [HSM17] HERMANS J., SPANAKIS G., MOECKEL R.: Accumulated gradient normalization. *ArXiv abs/1710.02368* (2017). 2, 4
- [HZRS16] HE K., ZHANG X., REN S., SUN J.: Deep residual learning for image recognition. *2016 IEEE Conference on Computer Vision and Pattern Recognition (CVPR)* (2016), 770–778. 3, 4
- [Iof17] IOFFE S.: Batch renormalization: Towards reducing minibatch dependence in batch-normalized models. In *NIPS* (2017). 2, 4, 6
- [KL17] KLOKOV R., LEMPITSKY V. S.: Escape from cells: Deep kd-networks for the recognition of 3d point cloud models. *2017 IEEE International Conference on Computer Vision (ICCV)* (2017), 863–872. 5
- [LBD17] LE T., BUI G., DUAN Y.: A multi-view recurrent neural network for 3d mesh segmentation. *Comput. Graph.* 66 (2017), 103–112. 1, 2
- [LBS*18] LI Y., BU R., SUN M., WU W., DI X., CHEN B.: Pointnet: Convolution on x-transformed points. In *NeurIPS* (2018). 1, 2, 6
- [LCL18] LI J., CHEN B. M., LEE G. H.: So-net: Self-organizing network for point cloud analysis. In *Proceedings of the IEEE conference on computer vision and pattern recognition* (2018), pp. 9397–9406. 6
- [LGB*11] LIAN Z., GODIL A., BUSTOS B., DAUDI M., HERMANS J., KAWAMURA S., KURITA Y., LAVOUÉ G., NGUYEN H. V., OHBUCHI R., OHKITA Y., OHISHI Y., PORIKLI F. M., REUTER M., SIPIRAN I., SMEETS D., SUETENS P., TABIA H., VANDERMEULEN D.: Shrec '11 track: Shape retrieval on non-rigid 3d watertight meshes. In *3DOR@Eurographics* (2011). 4
- [LT20] LAHAV A., TAL A.: Meshwalker: Deep mesh understanding by random walks. *ACM Trans. Graph.* 39 (2020), 263:1–263:13. 2, 5
- [MGA*17] MARON H., GALUN M., AIGERMAN N., TROPE M., DYM N., YUMER E., KIM V. G., LIPMAN Y.: Convolutional neural networks on surfaces via seamless toric covers. *ACM Transactions on Graphics (TOG)* 36 (2017), 1–10. 5
- [MLR*20] MILANO F., LOQUERCIO A., ROSINOL A., SCARAMUZZA D., CARLONE L.: Primal-dual mesh convolutional neural networks. *ArXiv abs/2010.12455* (2020). 2, 4, 5
- [QGY*22] QIAO Y.-L., GAO L., YANG J., ROSIN P. L., LAI Y.-K., CHEN X.: Learning on 3d meshes with laplacian encoding and pooling. *IEEE Transactions on Visualization and Computer Graphics* 28 (2022), 1317–1327. 3
- [QSMG17] QI C., SU H., MO K., GUIBAS L. J.: Pointnet: Deep learning on point sets for 3d classification and segmentation. *2017 IEEE Conference on Computer Vision and Pattern Recognition (CVPR)* (2017), 77–85. 1, 2, 5, 6
- [QYSG17] QI C., YI L., SU H., GUIBAS L. J.: Pointnet++: Deep hierarchical feature learning on point sets in a metric space. In *NIPS* (2017). 1, 2, 5, 6
- [RDGF16] REDMON J., DIVVALA S. K., GIRSHICK R. B., FARHADI A.: You only look once: Unified, real-time object detection. *2016 IEEE Conference on Computer Vision and Pattern Recognition (CVPR)* (2016), 779–788. 1
- [RFB15] RONNEBERGER O., FISCHER P., BROX T.: U-net: Convolutional networks for biomedical image segmentation. In *MICCAI* (2015). 3
- [RUG17] RIEGLER G., ULUSOY A. O., GEIGER A.: Octnet: Learning deep 3d representations at high resolutions. *2017 IEEE Conference on Computer Vision and Pattern Recognition (CVPR)* (2017), 6620–6629. 2
- [SACO22] SHARP N., ATTAIKI S., CRANE K., OVSJANIKOV M.: Diffusionnet: Discretization agnostic learning on surfaces. *ACM Trans. Graph.* 41, 3 (mar 2022). 1, 2, 3, 5

- [SMKLM15] SU H., MAJI S., KALOGERAKIS E., LEARNED-MILLER E. G.: Multi-view convolutional neural networks for 3d shape recognition. *2015 IEEE International Conference on Computer Vision (ICCV)* (2015), 945–953. [1](#), [2](#)
- [SOG09] SUN J., OVSJANIKOV M., GUIBAS L. J.: A concise and provably informative multi-scale signature based on heat diffusion. *Computer Graphics Forum* 28 (2009). [3](#)
- [SS21] SMIRNOV D., SOLOMON J. M.: Hodgenet: Learning spectral geometry on triangle meshes. *ACM Trans. Graph.* 40 (2021), 166:1–166:11. [2](#), [5](#)
- [TCA*17] TCHAPMI L. P., CHOY C. B., ARMENI I., GWAK J., SAVARESE S.: Segcloud: Semantic segmentation of 3d point clouds. *2017 International Conference on 3D Vision (3DV)* (2017), 537–547. [2](#)
- [UVL16] ULYANOV D., VEDALDI A., LEMPITSKY V. S.: Instance normalization: The missing ingredient for fast stylization. *ArXiv abs/1607.08022* (2016). [6](#)
- [VBMP08] VLASIC D., BARAN I., MATUSIK W., POPOVIĆ J.: Articulated mesh animation from multi-view silhouettes. *ACM SIGGRAPH 2008 papers* (2008). [5](#)
- [VSP*17] VASWANI A., SHAZEER N. M., PARMAR N., USZKOREIT J., JONES L., GOMEZ A. N., KAISER Ł., POLOSUKHIN I.: Attention is all you need. *ArXiv abs/1706.03762* (2017). [2](#), [4](#)
- [WAvK*12] WANG Y., ASAFI S., VAN KAICK O. M., ZHANG H., COHEN-OR D., CHEN B.: Active co-analysis of a set of shapes. *ACM Transactions on Graphics (TOG)* 31 (2012), 1 – 10. [5](#)
- [WDH*23] WOO S., DEBNATH S., HU R., CHEN X., LIU Z., KWEON I. S., XIE S.: ConvNeXt V2: Co-designing and Scaling ConvNets with Masked Autoencoders. *arXiv e-prints* (Jan. 2023), arXiv:2301.00808. [6](#)
- [WH18] WU Y., HE K.: Group Normalization. *arXiv e-prints* (Mar. 2018), arXiv:1803.08494. [6](#)
- [WQF19] WU W., QI Z., FUXIN L.: Pointconv: Deep convolutional networks on 3d point clouds. In *Proceedings of the IEEE/CVF Conference on computer vision and pattern recognition* (2019), pp. 9621–9630. [6](#)
- [WSK*15] WU Z., SONG S., KHOSLA A., YU F., ZHANG L., TANG X., XIAO J.: 3d shapenets: A deep representation for volumetric shapes. *2015 IEEE Conference on Computer Vision and Pattern Recognition (CVPR)* (2015), 1912–1920. [2](#)
- [WSLT18] WANG P.-S., SUN C.-Y., LIU Y., TONG X.: Adaptive O-CNN: A Patch-based Deep Representation of 3D Shapes. *ACM Transactions on Graphics (SIGGRAPH Asia)* 37, 6 (2018). [2](#)
- [XDZ17] XU H., DONG M., ZHONG Z.: Directionally convolutional networks for 3d shape segmentation. In *2017 IEEE International Conference on Computer Vision (ICCV)* (2017), pp. 2717–2726. [5](#)
- [XDZQ21] XU M., DING R., ZHAO H., QI X.: Paconv: Position adaptive convolution with dynamic kernel assembling on point clouds. In *Proceedings of the IEEE/CVF Conference on Computer Vision and Pattern Recognition* (2021), pp. 3173–3182. [6](#)
- [XFX*18] XU Y., FAN T., XU M., ZENG L., QIAO Y.: Spidercnn: Deep learning on point sets with parameterized convolutional filters. In *Proceedings of the European conference on computer vision (ECCV)* (2018), pp. 87–102. [6](#)
- [XZQ20] XU M., ZHOU Z., QIAO Y.: Geometry sharing network for 3d point cloud classification and segmentation. In *Proceedings of the AAAI Conference on Artificial Intelligence* (2020), vol. 34, pp. 12500–12507. [6](#)
- [YXKI20] YANG X., XIA D., KIN T., IGARASHI T.: Intra: 3d intracranial aneurysm dataset for deep learning. In *Proceedings of the IEEE/CVF Conference on Computer Vision and Pattern Recognition* (2020), pp. 2656–2666. [5](#), [6](#)
- [YZW*21] YU J., ZHANG C., WANG H., ZHANG D., SONG Y., XIANG T., LIU D., CAI W.: 3d medical point transformer: Introducing convolution to attention networks for medical point cloud analysis. *arXiv preprint arXiv:2112.04863* (2021). [5](#), [6](#)
- [ZFF*21] ZHOU H., FENG Y., FANG M., WEI M., QIN J., LU T.: Adaptive graph convolution for point cloud analysis. In *Proceedings of the IEEE/CVF international conference on computer vision* (2021), pp. 4965–4974. [6](#)